Accepted version. Personal use of this material is permitted. Permission from IEEE must be obtained for all other uses, in any current or future media, including reprinting/republishing this material for advertising or promotional purposes, creating new collective works, for resale or redistribution to servers or lists, or reuse of any copyrighted component of this work in other works. Copyright Owner: Institute of Electrical and Electronics Engineers; printed ISSN: 1530-437X; electronic ISSN: 1558-1748. DOI: 10.1109/JSEN.2017.2711643.

Fully Planar 4H-SiC Avalanche Photodiode with Low Breakdown Voltage

A. Sciuto, M. Mazzillo, P. Lenzi, S. Di Franco, D. Mello, P. P. Barbarino, G. Longo, S. Cascino, A. Santangelo, S. Albergo, A. Tricomi, O. Starodubtsev, O. Adriani, G. D'Arrigo.

Abstract— **We report on the structure and performance of 4H-SiC p^+-n APDs fabricated in fully planar technology. A dark current density lower than 10 nA/cm^2 at 30V reverse bias and a breakdown voltage of 88 V were observed. A gain as high as 10^5 was measured at 94 V reverse bias, confirming the avalanche multiplication working condition. The maximum responsivity value was measured at 270 nm, increasing from 0.06 A/W (QE=29%) at 0V bias to 0.10 A/W (QE of about 45%) at 30V reverse bias.**

Index Terms— **UV Detectors, 4H-SiC, APD Photodiodes, planar technology, shallow junction, ion implantation.**

I. Introduction

High sensitivity solid-state ultraviolet (UV) sensors find many applications in the industrial and consumer markets such as flame detection, deep-space UV astronomy, water purification, compound identification, non-line-of–sight UV communication and more recently biological or chemical agent detection [1,2]. Among the wide-bandgap based devices, 4H-SiC detectors are the best choice for all applications requiring high signal-to-noise ratio in presence of very low incident photon flux and visible light rejection. As well-known in fact, SiC devices are intrinsically characterized by very low leakage current and visible light blindness [3]. Moreover 4H-SiC is today suitable for microelectronic device and sensor fabrication, due to the high quality of the substrates and epitaxial layers and the mature processing technology [4]. UV sensitive SiC-based Avalanche Photodiodes (APDs) were proposed in literature by a couple of decades as replacement for standard photomultiplier tubes (PMTs) in many applications requiring at the same time high internal gain and very fast electro-optical response [5, 6].

Furthermore, with respect to PMTs, APDs are characterized by high compactness, insensitivity to magnetic fields and in perspective low cost, due to the solid-state approach. The majority of the SiC-APD devices disclosed in the literature are fabricated by using the epitaxial layer growth technique and mesa sidewall structures with very low bevel angles (Θ~4°) for the lateral confinement of the electrical field [2, 8].

A. Sciuto, S. Di Franco, and G. D'Arrigo are with CNR–IMM, Catania-Italy (e-mail: antonella.sciuto@imm.cnr.it; salvatore.difranco@imm.cnr.it; giuseppe.darrigo@imm.cnr.it).
M. Mazzillo, D. Mello, P.P. Barbarino, G. Longo, S. Cascino, A. Santangelo are with STMicroelectronics, Catania, Italy (e-mail: massimo.mazzillo@st.com; domenico.mello@st.com; pierpaolo.barbarino@st.com; peppe.longo@st.com; salvatore.cascino@st.com; antonello.santangelo@st.com).
P. Lenzi and O. Adriani are with INFN section of Firenze, Italy & with Physics Dept., University of Firenze, Italy (e-mail: lenzipi@fi.infn.it; oscar.adriani@fi.infn.it)
O. Starodubtsev is with INFN dep. of Firenze, Italy (e-mail: starodubtsev@fi.infn.it)
S. Albergo and A. Tricomi are with INFN section of Catania & with Physics Dept., University of Catania, Italy (e-mail: sebastiano.albergo@ct.infn.it; alessia.tricomi@ct.infn.it).

These detectors are characterized by a low fill factor due to the dead region all around the active area, arising from the use of the bevel structure. This is a fundamental limit for the fabrication of high density APD arrays. Moreover many of these devices have a breakdown voltage (BV) of a few hundreds of Volts, further limiting their use in many applications.

In the recent past we fabricated 4H-SiC Schottky photodiodes with Ni_2Si interdigitated and thin continuous metal film on the surface of the detectors [9-13]. 4H-SiC p^+-n detectors were also manufactured at a prototype level [14]. All these detectors operate without amplification and were characterized by a high detection efficiency in the full UV range obtained already at 0V bias, good visible light blindness and very low leakage current obtained on large area devices.

In this paper we report on the structure and performance of 4H-SiC p^+-n APDs fabricated in fully planar technology. The p^+ shallow region in the active area of the devices is defined by low energy implantation of Al^+ ions onto an n-type 4H-SiC epitaxial layer. A planar edge ring obtained through a deeper implanted p region surrounds the active area of the detectors to prevent the edge breakdown. This approach guarantees a significant increase of the geometrical fill factor up to a valuable of 65% in the proposed detector's structure (50 μm diameter of active area and 6 μm large lateral confinement structure) to be compared to the 35% or lower value of the devices disclosed in the literature (calculated for the same active area diameter and mesa lateral confinement structure 1.2 μm deep with a ~ 4° bevel angle) [7]. A dark current density lower than 10 nA/cm^2 was measured at 30V reverse bias (arbitrarily fixed as unit multiplication gain bias). The dark current increases significantly in avalanche multiplication region up to about 1 μA/cm^2 at a gain of 100, due to relevant injection of leakage current from the border of the devices. In spite of the high dark current, gain values as high as 10^5 have been measured at 94 V reverse bias, confirming the avalanche multiplication working condition.

Accepted version. Personal use of this material is permitted. Permission from IEEE must be obtained for all other uses, in any current or future media, including reprinting/republishing this material for advertising or promotional purposes, creating new collective works, for resale or redistribution to servers or lists, or reuse of any copyrighted component of this work in other works. Copyright Owner: Institute of Electrical and Electronics Engineers; printed ISSN: 1530-437X; electronic ISSN: 1558-1748. DOI: 10.1109/JSEN.2017.2711643.

II. Photodiode Fabrication and Structural Characterization

The SiC APDs devices were fabricated at STMicroelectronics-Catania and CNR-IMM-Catania clean room facilities using 4H-SiC epitaxial layers grown by LPE–Italy Silicon Carbide Epi Technologies on an n-type heavily doped (1×10^{19} donor/cm^3) 4H-SiC 4" diameter substrates.

A high dose and low energy Al^+ multiple implantation process was used to form the p^+ shallow layer in the n-doped epitaxial layer (1.2 µm thick, 5×10^{17} atoms/cm^3 doping) in the active area region. A higher energy Al^+ implantation process was used to define the p-doped edge ring all around the active area region. A dedicated high temperature thermal annealing process in Ar ambient was used to activate the dopant and recover the implantation damage [14]. The Ohmic contacts on the n^+ back substrate and on the p^+ top surface were formed by sputtering a 200 nm and 100 nm thick Ni film, followed by rapid annealing processes at 1000 °C and 750°C, respectively, in N_2 ambient to form Ni_2Si films [10-13]. The devices are laterally surrounded by a 1.6 µm thick TEOS (tetraethylorthosilicate) ring and aluminium contact pads were deposited on the front side for the anode region contact. We fabricated devices with circular geometry with an optically active open area (OAOA) diameter of 20, 50, 100, 200 and 500 µm (p^+ active area region directly exposed to the radiation). In this design no passivation layer was used on the front side of the devices, in order to minimize the optical losses due to the typical high absorption of the dielectric layers (e.g. Si_3N_4), especially for low wavelengths in the UV range [15].

A cross section scheme of the fabricated devices is reported in the left portion of Fig. 1. The p-type ring region is partially superimposed to the p^+ central active area region. Both the p type layers are coplanar and defined inside the same superficial n-type epitaxial layer. The TEOS layer surrounds the active area of the detector. The Ni_2Si surface metal layer partly overlaps the p^+ central region for the anode contact. Finally the Al contact pad layer is observable on the external portion of the device on top to the TEOS layer and, partially, on the Ni_2Si front ohmic contact layer. A top view optical microscopy image of one of the fabricated devices is shown in the right portion of Fig. 1: it is observable, in the bottom region of the picture, the circular metallic pad (diameter of 100 µm), and in the top, the circular device region with a central portion of the semiconductor device, directly exposed to the impinging radiation (20 µm internal diameter for this device).

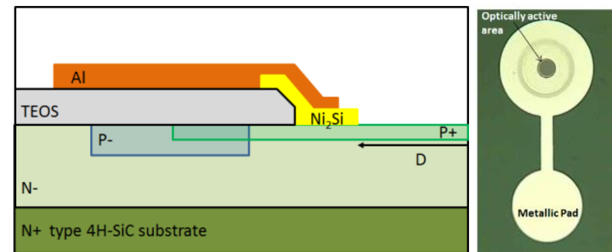

Fig. 1 Not in scale edge cross section scheme of a typical device (on the left side), and optical microscopy top view image of a device with optical active open area of 20 µm internal diameter (on the right side).

A structural characterisation of the fabricated devices was performed by FIB-FD analysis (Focused Ion Beam - Dual Beam) in order to evidence the shape, the lateral and vertical extension of the implanted regions and the morphology of the surrounding TEOS and Al metal layer. In Fig. 2, the cross section of the sample can be observed. In particular, into the FIB chamber, a very narrow strip of Tungsten was deposited on the surface of the cross section area that was used as contrast layer. In the inset of the Fig 2, as reference, is reported a picture of the device under test with a black dashed line that indicates the cross-section line, that was performed using FIB and observed by SEM (Scanning Electron Microscopy) mostly on the device's edge. In the upper portion of Fig. 2, a SEM image at low magnification is reported for showing an overview of the cut region. Instead in the lower portion of the same Fig. 2, a higher magnification image is reported in order to observe in details the area in the dashed box. The analysis shows how the lateral p type ring and the central p^+ active regions have a vertical extension of about 1 µm and 380 nm, respectively. Both these values are compatible with the implanted regions depth values estimated by device processing simulation (SILVACO® software) not shown here for brevity. The TEOS layer, 1.6 µm thick, shows a trapezoidal shape at the borders of the device, due the under mask etch occurred during the wet etch processing used for its definition. A very thin Ni_2Si layer is visible on the active area of the device. The Al layer, 1 µm thick, exhibits different grain sizes on the device structure, in particular on the TEOS layer at the device's edge. This could be due to the interaction of the aluminium metal layer with a very thin Ni layer on the TEOS not silicidized during the annealing process used for the Ni_2Si formation.

Accepted version. Personal use of this material is permitted. Permission from IEEE must be obtained for all other uses, in any current or future media, including reprinting/republishing this material for advertising or promotional purposes, creating new collective works, for resale or redistribution to servers or lists, or reuse of any copyrighted component of this work in other works. Copyright Owner: Institute of Electrical and Electronics Engineers; printed ISSN: 1530-437X; electronic ISSN: 1558-1748. DOI: 10.1109/JSEN.2017.2711643.

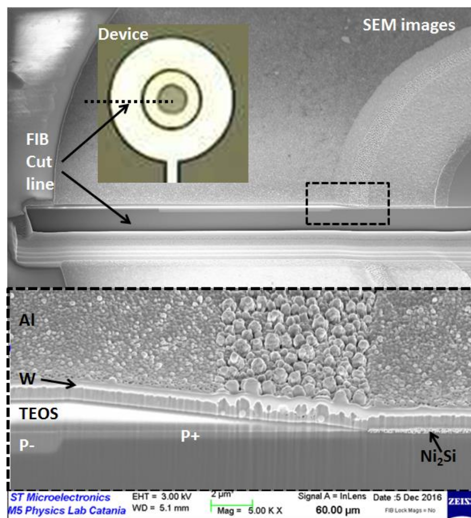

Fig. 2 SEM images of a fabricated device. On the left up region an optical microscopy image of the device is reported as reference, with the dashed black line that indicates the FIB cutting line. The low and high magnification SEM images are in the upper and lower portion of the figure, respectively.

III. Electro-optical characterization

The IV characteristics of the diodes were measured on wafer, on a large number of devices, in dark condition using a probe station and a semiconductor parameter analyser (Agilent 4155C). The characterization results here reported are focused on the APDs with smaller active area for their relatively lower dark current. The IV forward characteristics of three typical devices with 20, 50 and 100 µm active area diameter are shown in Fig. 3, while the reverse characteristics measured on the same devices are reported in Fig.4. In agreement with literature data [16, 17], the devices exhibit rectifying IV characteristic with a sharp turn-on at relatively high threshold voltage (about 1.6 V) and current dominated by carrier diffusion in the under threshold region and by recombination at higher bias. Series resistance effects are visible in the IV forward characteristics at voltage higher than about 2.7 V [16-18]. Low leakage (dark) currents were measured at low reverse bias with current density of about 10 nA/cm^2 at 30 V. The dark current increases rapidly for higher reverse bias exceeding 50 V up to reach the breakdown voltage around 88 V.

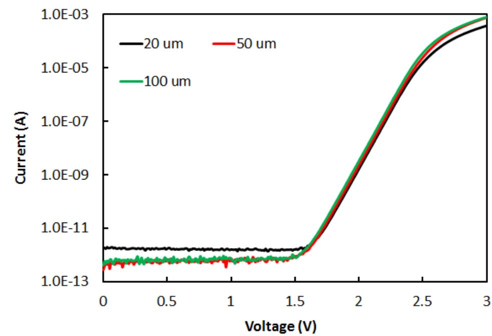

Fig. 3. IV forward characteristics of three typical APDs with active area diameters of 20, 50 and 100 µm measured on wafer in dark and room temperature conditions.

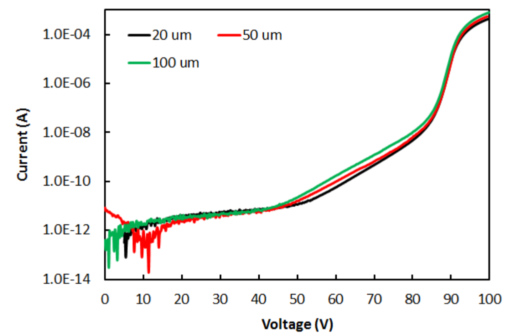

Fig. 4. IV reverse characteristics of three typical APDs with active area diameters of 20, 50 and 100 µm measured on wafer in dark and room temperature conditions. The forward characteristics measured on the same devices are reported in Fig.3.

An UV Xenon lamp was used as a broadband light source to measure the photocurrent under white light illumination. The I-V reverse characteristics measured on a typical 50 µm diameter APD in dark and white light illumination conditions, are superimposed in Fig. 5 (current values shown on the left vertical axis). In the same figure on the vertical right axis, is reported the multiplication gain estimated at the same reverse bias values by using the following relation [19]:

$$Gain = (I_{ph} - I_{dark})/(I_{ph_@30V} - I_{dark_@30V}) \quad (1)$$

where I_{ph} and I_{dark} are the currents measured under illumination (photocurrent) and in dark conditions, respectively. Here, the reference unit gain was arbitrary defined at 30 V reverse bias; this voltage value was fixed well below the voltage value at which the impact ionization becomes significant. The photocurrent, dark current and Gain values for several operation voltage values below and above the BV, are also summarised in Table 1 : Gain values of 10^2 and 10^5 are measured at 88 and 94 V, respectively, confirming the avalanche multiplication working condition, in spite of the fact that the high leakage current injection makes soft the current onset at the BV. Obtained values are comparable, within experimental error, to those of similar

Accepted version. Personal use of this material is permitted. Permission from IEEE must be obtained for all other uses, in any current or future media, including reprinting/republishing this material for advertising or promotional purposes, creating new collective works, for resale or redistribution to servers or lists, or reuse of any copyrighted component of this work in other works. Copyright Owner: Institute of Electrical and Electronics Engineers; printed ISSN: 1530-437X; electronic ISSN: 1558-1748. DOI: 10.1109/JSEN.2017.2711643.

devices already in the market or disclosed in the literature [5, 19, 20].

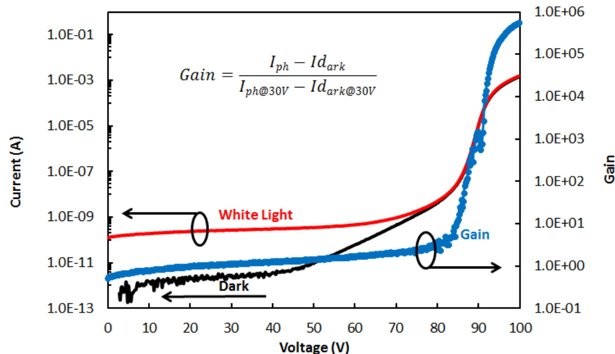

Fig. 5 IV reverse characteristics measured on a typical 50 µm active area diameter APD in dark condition and under white light illumination. The current is reported on vertical left axis. The multiplication gain obtained through the formula reported in inset, assuming 30 V value as reference unit gain bias, is reported on the vertical right axis.

Table I
Obtained Gain values of a typical 50 µm active area diameter APD.

Operation Voltage (V)	I_{ph} (A)	I_{dark} (A)	Gain
30	2.71E-10	2.85E-12	1
80	9.94E-09	4.14E-09	3
88	6.19E-07	5.27E-07	3.43E+02
94	3.48E-04	3.17E-04	1.15E+05

The dark IV characteristics of devices with different active area diameters were also analysed to estimate the surface/peripheral and bulk components of the dark current, as described in previous literature works for similar devices [21]. To this purpose we plotted in Fig.6 the dark current values measured at fixed reverse biases of 20 V and 80 V on APDs with active area diameter (D) of 20, 50, 100, 200 and 500 µm. The following equation was used to fit the experimental data:

$$I_{total} = j_{surface}.\pi.D + J_{bulk}.\pi.\left({}^{D}/_{2}\right)^{2} \quad (2)$$

where I_{total} indicates the device current, $j_{surface}$ is the surface/peripheral linear current density component expressed in A/cm and the J_{bulk} is bulk current density component expressed in A/cm^2. Equation (2) was used for the polynomial best fit of the experimental values (solid black lines superimposed to the experimental points in Fig. 6).

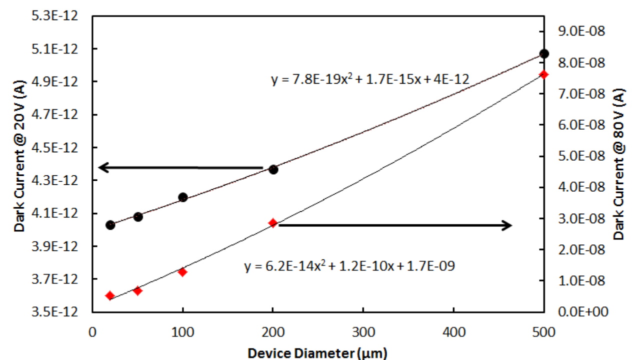

Fig. 6 Dark current values, measured at fixed reverse biases of 20 V (left vertical axis) and 80 V (right vertical axis) on APDs with 20, 50, 100, 200 and 500 µm active area diameters. Experimental points were fitted with polynomial curves (continuous lines): the obtained equations and relative correlation coefficients R^2, are reported in the figure.

The $j_{surface}$ and J_{bulk} values determined through the best fit were used to calculate in the equation 2 the peripheral and bulk contribution of the dark current for the tested devices at the two considered reverse bias values [19, 21]. An average surface contribution to the total dark current of about 93% and 88% was determined at 20 and 80 V, confirming the significant injection of leakage current from the borders of the devices.

Emission Microscopy (Em.Mi.) analyses are usually used to investigate microelectronic device faults and defects. Em.Mi. images generally report, in an intensity colour scale, the photon emission in a wide optical range from the near UV to the near infrared, due to hot electrons or to electron-hole pairs recombination inside the observed device. Em.Mi. measurements were performed on our APDs devices to obtain time integrated photon emission maps and then to evidence the regions of more intense electrical field through the observation of photons emitted by electron-hole recombination processes [22]. Em.Mi. analyses were carried out in dark condition using a Hamamatsu PHEMOS-1000 Emission Microscope equipped with a Si-CCD camera (C4880-01 model) cooled at -50°C in operation condition.

In the following, the emission analyses are superimposed to the optical microscopy images acquired on the device under test. An integration time of 50 s was used for all the Em.Mi. acquisitions. In Fig. 7 the Em.Mi. measured at room temperature on an APD with 50 µm active area diameter are shown at increasing reverse bias, close to the BV in a typical color temperature scale (i.e. red colour corresponds to a more intense emission). The pictures can be regarded as snapshots of successive phases of the turn-on transient in the active area of the device. A relevant increase of photons emission from the central active area is observed from 87.5 V to 89.5 V reverse bias. Certainly, photons generated under the metal region (that appears in white colour in the Em.Mi. images) are absorbed by the overlying layers. In any case from the more intense light emission, we can deduce that the avalanche

Accepted version. Personal use of this material is permitted. Permission from IEEE must be obtained for all other uses, in any current or future media, including reprinting/republishing this material for advertising or promotional purposes, creating new collective works, for resale or redistribution to servers or lists, or reuse of any copyrighted component of this work in other works. Copyright Owner: Institute of Electrical and Electronics Engineers; printed ISSN: 1530-437X; electronic ISSN: 1558-1748. DOI: 10.1109/JSEN.2017.2711643.

multiplication starts in the detector's active area, as desired.

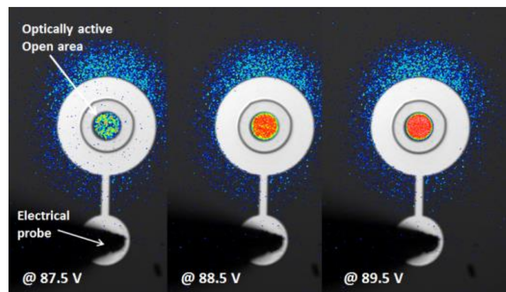

Fig. 7 Em.Mi. images of a 50 µm APD (50 s integration time). Images are in intensity colour scale with red and blue colours indicating a higher and lower photons intensity emission, respectively.

The APD's optical characterization was completed through responsivity and photocurrent measurements performed on wafer by using a Xenon lamp, a CVI/Digikrom DK240 monochromator, a 100 µm diameter core optical fiber provided with focusing system and a commercial Ophir-Optronics power meter, used to calibrate the apparatus [9-11]. The photocurrent curves measured on a 50 µm active area diameter device at 220, 250, 280, 310, 340, 370 and 600 nm illumination wavelengths are shown in Fig. 8 as a function of the reverse bias, compared also to the reverse current characteristic measured in dark condition on the same detector. As expected, the photocurrent curve measured in the visible range at 600 nm coincides with the dark one, due to the high intrinsic visible light blindness of the detector.

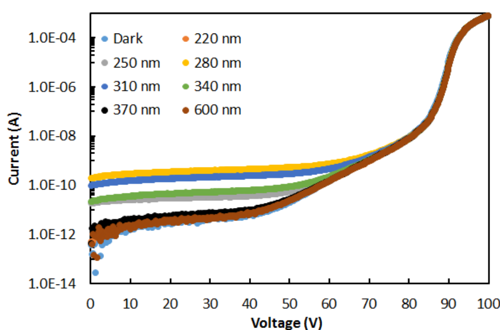

Fig. 8 Dark and photocurrents measured at different illumination wavelengths as a function of the reverse voltage on an APD with 50 µm active area diameter.

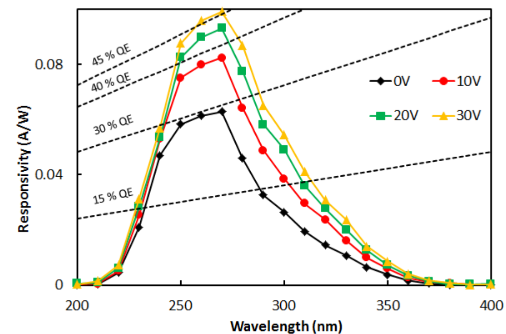

Fig. 9 Responsivity spectra measured as a function of the reverse voltage on an APD with 50 µm active area diameter. Theoretical responsivity lines at fixed QE values are also plotted.

The responsivity on the same device was measured at increasing reverse bias below the BV in the wavelength range between 200 and 400 nm. The measured values versus wavelength are reported in Fig. 9 along with the corresponding quantum efficiency (QE) dashed lines, calculated at four fixed reference values [23]. A relevant maximum responsivity was measured already at 0 V bias in the short wavelength range, due to the shallow junction layer technology and reduced dead layer thickness above the space charge region. A maximum responsivity of 0.06 A/W was obtained at 270 nm, corresponding to a QE of about 29 %. At increasing bias values, the responsivity significantly increases due to the increase of depletion layer thickness. A maximum value of 0.10 A/W (QE of about 45 %), was measured at 30 V reverse bias, a value very near to literature data reported for similar devices (QE of 44% in Ref. 19 and of 66 % in Ref. 5).

CONCLUSIONS

In this paper we reported on the performances of p^+-n 4H-SiC APDs fabricated in fully planar technology. The shallow p+ layer in the active area region and the p-type edge region for the electrical field confinement were obtained through suitable multiple Al^+ ions implantation steps on the n-type superficial epitaxial layer. The devices were structurally characterised by FIB-SEM microscopy while the electro-optical characteristics were investigated through responsivity and I-V characteristics measured in dark and under illumination condition. The detectors are characterized by a low leakage current in their linear operation range (dark current density lower than (< 10 nA/cm^2 at 30 V reverse bias). A gain value of 10^5 was extracted at 94 V, i.e. at 6 V above the estimated BV (88 V). The maximum responsivity value was measured at 270 nm, increasing from 0.06 A/W (QE=29%) at 0V bias to 0.10 A/W (QE of about 45%) at 30V reverse bias. From the analyses of the trend of dark current versus the device diameter at two fixed reverse biases (20 V and 80 V), a significant contribution of the surface/peripheral current to the total measured dark current was estimated. The

Accepted version. Personal use of this material is permitted. Permission from IEEE must be obtained for all other uses, in any current or future media, including reprinting/republishing this material for advertising or promotional purposes, creating new collective works, for resale or redistribution to servers or lists, or reuse of any copyrighted component of this work in other works. Copyright Owner: Institute of Electrical and Electronics Engineers; printed ISSN: 1530-437X; electronic ISSN: 1558-1748. DOI: 10.1109/JSEN.2017.2711643.

edge ring region will be optimized in next fabrication runs in order to reduce the injection of the leakage current from the borders of the devices.

REFERENCES

[1] G.A. Shaw et al., “Recent progress in short-range UV communication”, *Proc. SPIE, vol. 5796, pp. 214–225, 2005.*
[2] H. Liu, D. McIntosh, X. Bai, H. Pan, M. Liu, J. C. Campbell, and H. Y. Cha, “4H-SiC PIN recessed window avalanche photodiode with high quantum efficiency,” *IEEE Photon. Technol. Lett.*,vol. 20, no. 18, pp. 1551–1553, 2008.
[3] F. Yan, Y. Luo, J. H. Zhao, and G. H. Olsen, “4H-SiC visible blind and UV avalanche photodiodes,” *Electron. Lett., vol. 35, no. 11, pp. 929–930, 1999.*
[4] X. She et al., “Review of Silicon Carbide Power Devices and Their Applications”, *IEEE Transactions on Industrial Electronics, vol. pp, 99, 2017.*
[5] L Li et al., “High Fill-Factor 4H-SiC Avalanche Photodiodes With Partial Trench Isolation” *IEEE Photonics Technology Letters, vol. 28, 22, 2016.*
[6] G.A. Shaw et al., “Deep UV Photon-Counting Detectors and Applications*”, Proc. SPIE 7320, Advanced Photon Counting Techniques III, 73200J , 2009; doi:10.1117/12.820825.*
[7] Dong Zhou et al., “High-Temperature Single Photon Detection Performance of 4H-SiC Avalanche Photodiodes”, *IEEE Photonics Technology Letters, vol. 26, 11, pp.1136-1138 June, 2014.*
[8] http://www.gano-uv.com/en/products.asp?bigId=91
[9] A. Sciuto et al., “High responsivity 4 H-Si C Schottky UV photodiodes based on the pinch-off surface effect”, *Applied physics letters 89 (8), 081111, 2006.*
[10] M. Mazzillo et al., “Highly Efficient Low Reverse Biased 4H-SiC Schottky Photodiodes for UV-Light Detection”, *IEEE Photonics Technology Letters, vol. 21, 1782-1784, 2009.*
[11] M.Mazzillo et al., “Temperature and Light Induced Effects on the Capacitance of 4H-SiC Schottky Photodiode”, *IEEE Sensors Journal vol. 12, 5, 1127-1130, 2012.*
[12] A. Sciuto et al., “Thin metal film Ni_2Si/4H–SiC vertical Schottky photodiodes”, *IEEE Photonics Technology Letters, vol. 26, 17, pp. 1782-1785, 2014.*
[13] M. Mazzillo et al., “Electro-Optical characterization of patterned thin metal film Ni_2Si-4H SiC Schottky photodiodes for UV light detection”, *IEEE Sensors Journal, vol. 15, 3, pp. 1858-1863, 2015.*
[14] A. Sciuto et al., “Visible blind 4H-SiC P+-N UV photodiode obtained by aluminum implantation”, *IEEE Photonics Journal, vol. 7, 3, 6801906, 2015.*
[15] A. Sciuto et al., “UV-A Sensor Based on 6H-SiC Schottky Photodiode*”, IEEE Photonics Journal, vol. 9, 1,pp. 1-10, 2017*
[16] S. M. Sze, Kwok K. Ng, *Physics of Semiconductor Devices*, Wiley Interscience, 1981, ISBN-13: 978-0-47 **1-1** 4323-9 ISBN-10: 0-471-14323-5.
[17] B.J. Baliga, *Fundamental of Power Semiconductor Devices*, *Spinger, 2008, ISBN 978-0-387-47313-0.*
[18] M.E. Dunn, “Electrical Characterization of 4H-SiC p-n junction diodes”, *PhD thesis, http://www.dtic.mil/dtic/tr/fulltext/u2/a309857.pdf*
[19] Q. Zhou, et al., “Proton-implantation-Isolated 4H-SiC avalanche Photdiodes”, *IEEE Photonics Technology Letters, vol.21, 23, pp.1734-1736, 2009.*
[20] L. Fei et al., “Discrimination voltage and overdrive bias dependent performance evaluation of passively quenched SiC single-photon-countin avalanche photodides”, *Chin. Phys. Lett. vol. 32,no. 8, 088503, 2015.*
[21] J. C. Campbell et al., “Recent advances in avalanche photodiodes”, *IEEE J. Sel. Topics Quantum Electron., vol. 10, no. 4, p. 777,Jul./Aug. 2004.*
[22] http://www.hamamatsu.com
[23] B.E.A. Saleh, M.C. Teich, *Fundamental of Photonics*, John Wiley & Sons, Inc., New York.